Three-dimensional X-ray Crystal Structure Analysis of Solution-processed Oriented Thin Film utilizing Liquid-crystalline Phthalocyanine

Masashi Ohmori, Mitsuhiro Nakatani, Masaya Kurokawa, Akihiko Fujii* and Masanori Ozaki
Division of Electrical, Electronic and Information Engineering, Graduate School of Engineering, Osaka University, Suita, Osaka 565-0871, Japan
*E-mail: afujii@opal.eei.eng.osaka-u.ac.jp

ABSTRACT

Molecular alignment control of non-peripherally hexyl-substituted phthalocyanine ($C6PcH_2$) in thin films has been investigated. Planar alignment of $C6PcH_2$ molecules in the thin film was induced by bar-coating, and homeotropic alignment was induced by the thermal annealing of $C6PcH_2$ thin film covered with a poly(vinylphenol) layer. The three-dimensional molecular packing structure in the uniaxially planar oriented thin film was clarified by the grazing incidence wide-angle X-ray scattering (GIWAXS) technique with sample rotation. The quality of the molecularly oriented thin film was discussed based on the X-ray rocking curve measurement and simulation utilizing the single-crystal structure of $C6PcH_2$. The molecular alignment in the homeotropically oriented thin film was also clarified by the temperature controlled GIWAXS measurement. The origin of inducing homeotropic alignment in the thin film was discussed based on the molecular alignment in the LC phase.

Keywords: molecular alignment control, GIWAXS, discotic liquid crystal, phthalocyanine, molecularly orientated thin film

1. INTRODUCTION

Phthalocyanines (Pcs) are well known as the low-molecular-weight semiconductors and disk-shaped molecules with π-conjugated macrocycle systems. Pcs tend to form the molecular stacking structure, and some of them exhibit high carrier mobility along the molecular stacking direction [1],[2]. Organic devices utilizing Pcs, such as solar cells and transistors, have been investigated [3],[4],[5]. Recently, solution-processable devices have been strongly desired because of potentials for the mass production and low equipment cost [6]. However, unsubstituted Pcs have a low solubility in typical organic solvents, and a uniform thin film cannot be obtained by the solution process.

To improve solubility in organic solvents, introducing alkyl-substituents to the non-peripheral position of Pcs has been investigated [7]. Some of non-peripheral alkyl-substituted Pcs exhibit the discotic liquid-crystalline (LC) phase and tend to form the columnar structure in the crystal phase [8]. The columnar structure is appropriate for the device applications because of the efficient carrier transport along the column axis. Actually, some of non-peripheral alkyl-substituted Pcs exhibit high carrier mobility over 10^{-1} cm^2/Vs [9]. Especially, non-peripheral hexyl-substituted Pc, 1,4,8,11,15,18,22,25-octahexylphthalocyanine ($C6PcH_2$) exhibits high hole and electron mobilities of 1.4 and 0.5 cm^2/Vs, respectively [10]. In addition, a crystallinity of $C6PcH_2$ is maintained in the spin-coated films [11], and $C6PcH_2$-based solar cells prepared by spin-coating have been reported to exhibit high power conversion efficiency of 4.2 % [12],[13]. The spin-coated thin films consist of non-oriented polycrystals of $C6PcH_2$. $C6PcH_2$ should exhibit electrical anisotropy [14],[15],[16]; therefore, molecular alignment control in the thin film is necessary to obtain high device performance.

Molecular alignment of $C6PcH_2$ in thin films is classified into two types: planar and homeotropic alignments. Uniaxial planar and homeotropically oriented thin films exhibit a high carrier mobilities in the direction parallel and perpendicular to the substrate, respectively. Hence, uniaxial planar and homeotropically oriented thin films are suitable for transistor and solar cell applications, respectively. Therefore, molecular alignment control of $C6PcH_2$ should be developed for the device applications.

Uniaxial planar alignment of $C6PcH_2$ in thin films has been realized by unique techniques such as heated spin-coating [17],[18] and contact freezing method utilizing the supercooled LC state [19],[20]. By these methods, uniaxial

Emerging Liquid Crystal Technologies XIII, edited by Liang-Chy Chien, Dirk J. Broer, Igor Muševič, Vladimir G. Chigrinov,
Proc. of SPIE Vol. 10555, 105550D · © 2018 SPIE · CCC code: 0277-786X/18/$18 · doi: 10.1117/12.2288083

planar oriented thin films were fabricated in the LC phase of $C6PcH_2$; however, undesired cracks generated in the films in the cooling process, because of the volumetric shrinkage, resulting in prohibiting the carrier transport. For avoiding such a problem, it is necessary to fabricate uniaxial planar oriented thin films at room temperature. Uniaxial planar oriented thin films of discotic LC semiconductors have been reported using printing methods, such as a zone-casting method [21]. In the zone-casting method, the direction and speed of the crystal growth could be controlled, and uniformly oriented crystals grow in the films. In this study, uniaxially planar oriented thin films of $C6PcH_2$ were fabricated by a bar-coating method, which is the similar approach to the zone-casting method.

Homeotropic alignment of $C6PcH_2$ has also been realized by using a conventional sandwich-cell structure with two glass plates, used for LC display devices [22],[23]. This process uses the unique properties of discotic LC semiconductors, which tend to exhibit homeotropic alignment without air interface [24]. In this process, the glass-sandwich cells are necessary and it is not suitable for the mass production. Homeotropic alignment in thin films prepared by the wet process, such as spin-coating and bar-coating, is desired. Homeotoropically oriented thin films prepared by the wet process have been proposed by using a polymer layer instead of the glass substrate [25]. The alignment mechanism seems to be similar as that of the sandwich-cell type devices, and this process must be effective for $C6PcH_2$.

For analyzing molecular orientation and packing structure in the thin films, X-ray diffraction (XRD) technique is generally used. Recently, XRD analysis utilizing a two-dimensional (2D) detector has been carried out, because of the availability of synchrotron radiation facilities, such as SPring-8, and development of semiconductor detectors [26]. The XRD measurement utilizing the 2D detector must be suitable to measure a 2D periodic structure, i.e., samples without azimuthal dependence, such as molecular oriented spin-coated [11] or vapor-deposited films [26]. Though the molecular packing structure in the uniaxially planar oriented thin films must be ordered three-dimensionally (3D) like a single-crystal, the analysis method for 3D oriented thin films is yet to be established.

In this study, uniaxial planar and homeotoropic alignments of $C6PcH_2$ in thin films were induced. The 3D molecular packing structure in the thin films were investigated by the grazing incidence wide-angle X-ray scattering (GIWAXS) technique with the sample rotation. The XRD patterns were discussed based on the simulation of the XRD patterns.

2. EXPERIMENTAL METHODS

2.1 Uniaxially planar alignment

Figure 1 shows the molecular and column structures of $C6PcH_2$, which was synthesized by a previously reported procedure [27]. The thin films were fabricated in the following manner. Glass substrates were cleaned with water, chloroform, acetone, and isopropyl alcohol by ultrasonication and then treated with UV-ozone. $C6PcH_2$ layers were prepared by bar-coating on the glass substrate. A schematic diagram of the bar-coating process is shown in Fig. 2 (a). A 9.6-mm-diameter coating bar, around which a 0.05-mm-diameter metal wire was wound, was fixed on the glass substrate. $C6PcH_2$ was dissolved in *p*-xylene at a concentration of 60 g/L, and the solution was added dropwise onto the coating bar, and then the glass substrate was moved in the horizontal direction at a speed of 30 μm/s. A small amount of the solution passed thorough the space between the wound metal wire and the glass substrate, resulting in the formation of a uniform film. The film thickness was estimated to be approximately 170 nm by an atomic force microscope (KEYENCE VN-8000 and Digital Instruments Nanoscope IIIA). Polarizing optical microscopy (POM) images were obtained with a polarized optical microscopy system (Nikon Eclipse LV 100 POL).

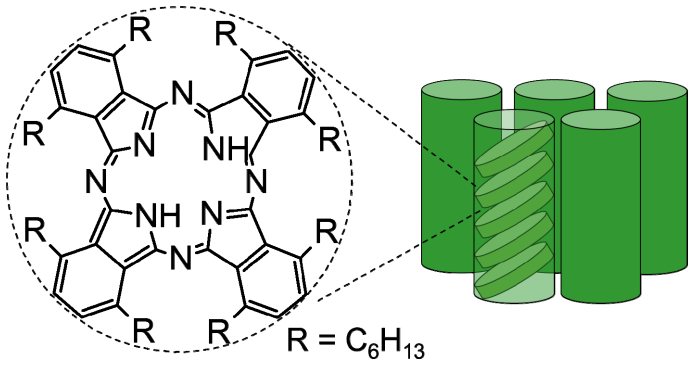

Figure 1. Molecular and column structure of $C6PcH_2$.

The GIWAXS measurement was carried out at room temperature in the BL46XU beamline at SPring-8 with the approval of JASRI (No. 2016A1776). The schematic diagram of the GIWAXS measurement setup is shown in Fig. 2(b). The X-ray diffraction was detected with a 2D detector (Dectris PILATUS 300K) equipped on a Huber eight-axis diffractometer. The wavelength of the X-rays was 1.0 Å and the incident angle was 0.12º. The GIWAXS measurement was carried out, while the thin film was rotated counterclockwise at a speed of 24º/min.

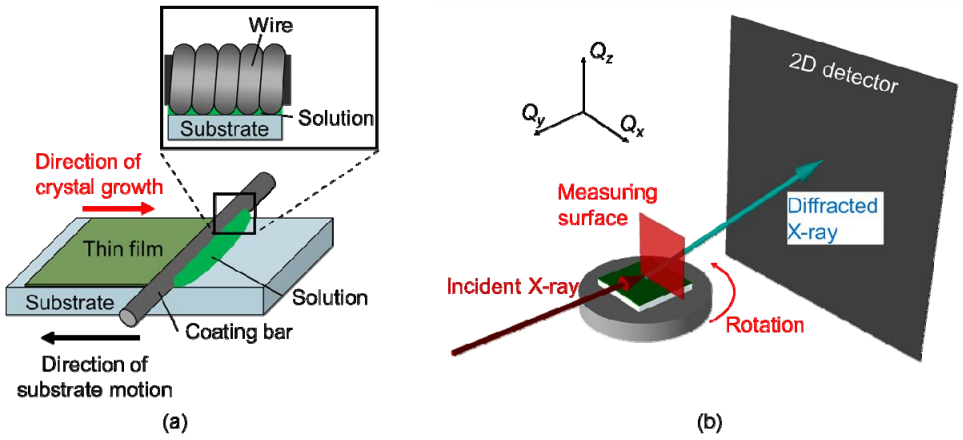

Figure 2. Schematic diagrams of (a) bar-coating process and (b) the GIWAXS measurement setup.

Calculation of XRD patterns were carried out in the following manner. First, the reciprocal lattice vector G was calculated by

$$\boldsymbol{G} = h\boldsymbol{a}^* + k\boldsymbol{b}^* + l\boldsymbol{c}^*, \tag{1}$$

where, h, k, and l are Miller indices, and $\boldsymbol{a}^*$, $\boldsymbol{b}^*$, and $\boldsymbol{c}^*$ are basic reciprocal lattice vectors. The coordinates of the reciprocal lattice points (G_x, G_y, G_z) were calculated by

$$G_x = 2\pi\frac{h}{a}, \tag{2}$$

$$G_y = 2\pi\frac{k}{b}, \tag{3}$$

$$G_z = \frac{2\pi}{\sin\beta}\left(\frac{l}{c} - \frac{h}{a}\cos\beta\right), \tag{4}$$

where, a, b, c, α, β, and γ are the unit-cell parameter. In the simulation, the analyzed data of the $C6PcH_2$ single-crystal, which has a monoclinic structure with a space group $P2_1/n$, a = 20.7430, b = 9.7984, c = 36.0961 Å, α = 90, β = 93.8750, and γ = 90º [28]. Intersection points of the reciprocal lattice vector and Ewald sphere are calculated by

$$\varphi = \cos^{-1}\frac{\lambda(G_x^2 + G_y^2 + G_z^2)}{4\pi\sqrt{G_x^2 + G_y^2}} - \tan^{-1}\frac{G_x}{G_y}, \tag{5}$$

where, φ is the rotation angle of the measured sample. From these equations, the positions of the XRD peaks can be calculated. The peak intensity was calculated by using the powder XRD analysis software (RIGAKU PDXL 2.6). The shape of the peak in the simulation was postulated to possess a normal distribution with the standard deviation, which was assumed to be 0.01 nm^{-1} in the $Q_{x,y}$-Q_z plane and 2º in the azimuthal direction. Here, $Q_{x,y}$ and Q_z are the wavenumbers in the in-plane and out-of-plane directions of the bar-coated thin film, respectively. Q_y is the wavenumber in the direction parallel to the sweep direction shown in Fig. 2(b). Relative factor R_F was calculated to evaluate the difference between measured and measured peak intensities, and R_F was calculated by

$$R_F = \frac{\sum\left||F_M| - |F_C|\right|}{\sum|F_M|} \times 100, \tag{6}$$

where, F_M and F_C are the measured and calculated values of the peak intensity.

2.2 Homeotropic alignment

The thin films were fabricated in the following manner. Glass substrates were cleaned with an alkaline solution (Furuuchi Chemical Semico Clean 56) and water by ultrasonication, then treated with UV-ozone. $C6PcH_2$ was dissolved in chloroform at a concentration of 60 g/L, and the solution was spin-coated onto the glass substrates at a speed of 500 rpm. The film thickness was estimated to be approximately 450 nm by the optical absorption measurement of spectrophotometry (Shimazu UV-3150). PVP (Aldrich Mw 25,000) was dissolved in methanol at a concentration of 40 g/L, and the solution was spin-coated onto the $C6PcH_2$ layer at the speed of 3000 rpm. The film thickness was estimated to be approximately 160 nm by a surface profilometer (Veeco DEKTAK 150). The sample was heated to 175 ºC in the isotropic phase of $C6PcH_2$ at a rate of 20 ºC/min, and cooled down to room temperature at a rate of 10 ºC/min.

The GIWAXS measurements were carried out in the BL46XU and BL18B2 beamlines at SPring-8 with the approvals of JASRI (No. 2016A1776 and 2017B1745). The wavelength of the X-ray was 1.0 Å and the incident angle was 0.12º. A 2D detector was used as an X-ray detector. The GIWAXS measurement was carried out at room temperature under atmospheric pressure or at 160 ºC under a pressure of approximately 10^{-3} Pa.

3. RESULTS AND DISCUSSIONS

3.1 Uniaxially planar alignment

Figure 3 shows typical POM images of the $C6PcH_2$ thin film prepared by bar-coating when the angles between the polarizer and the sweep direction of the wire-bar are 0 and 45º. These images were uniformly bright and dark at the diagonal and extinction positions, respectively. The POM images show that the uniform and uniaxial molecularly oriented thin film was obtained by bar-coating in an area of approximately 1 mm^2. Some horizontal lines were observed in the POM image at the diagonal position. Thus, the bar-coated thin film consisted of molecularly oriented poly-crystals of $C6PcH_2$. The domain boundaries should be caused by the difference between the crystal growth rate and the sweep speed of the wire-bar. The optimization of the fabrication condition such as the sweep speed of the wire-bar, organic solvents and fabrication temperature is necessary to obtain the single-crystalline thin films.

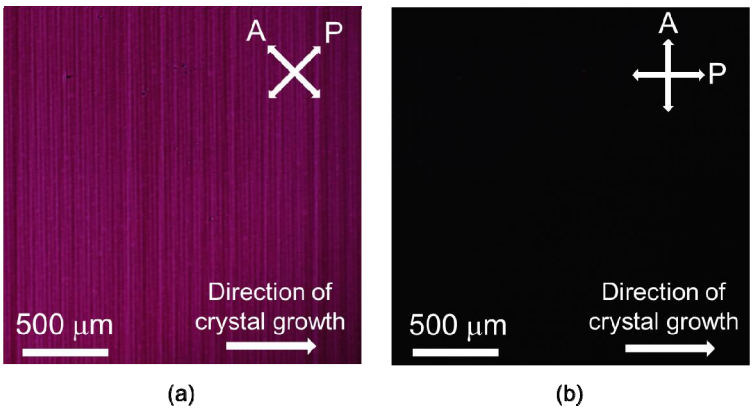

Figure 3. POM images of the $C6PcH_2$ thin film prepared by bar-coating at the (a) diagonal and (b) extinction positions.

Figure 4 shows XRD patterns obtained in the GIWAXS measurement, when the thin film was rotated in the counterclockwise direction by 0º, 30º, 60º, 90º, 120º, and 150º, as shown in Fig. 2(b). For all XRD patterns, spotty peaks were detected. The diffraction pattern from a randomly oriented powder is circular, because of the averaging of the diffracted intensity at equal scattering angles. The spotty peaks indicate that $C6PcH_2$ are aligned on the glass substrate. In Fig. 4(a), an XRD peak was detected at ($Q_{x,y}$, Q_z) = (0, 3.52) (nm^{-1}) (17.8 Å), which corresponds to the (002) plane of the single-crystal structure of $C6PcH_2$. The result shows that the (002) plane was parallel to the glass substrate. Moreover, periodic XRD peaks were detected at $Q_{x,y}$ = 3.10 nm^{-1} (20.2 Å) in the in-plane direction. The periodic XRD peaks correspond to the lattice constant a (20.7 Å) of the single-crystal structure of $C6PcH_2$. Thus, the a axis of $C6PcH_2$ in the bar-coated films is parallel to the in-plane direction. In Figs. 4(c) and 4(d), strong peaks based on the (12l) (l = -7, -6, -5, 5, 6) planes were detected at ($Q_{x,y}$, Q_z) = (13.2, 9-12) (nm^{-1}). These diffraction surfaces almost correspond to the periodic surfaces based on the inter-core distance of $C6PcH_2$. These results indicate that the molecular stacking direction of $C6PcH_2$ in the bar-coated thin films is almost parallel to the Q_y axis. The b axis of the single-crystal structure of $C6PcH_2$ was parallel to the molecular stacking direction [28], i.e., the b axis should be parallel to the Q_y axis. From these results, the 3D molecular alignment of $C6PcH_2$ in the bar-coated thin film was determined. To summarize, the Q_x, Q_y, and Q_z axes correspond to the a, b, and c axes of the single-crystal structure of $C6PcH_2$, respectively. Miller indices calculated by Eqs. (2), (3), and (5) are shown in Fig. 4. The measured peak positions are agreed with the calculated ones.

Figure 5 shows the simulated XRD patterns using the single-crystal structure by Eqs. (2)-(5) when the thin film was rotated in the counterclockwise direction by 0º, 30º, 60º, 90º, 120º, and 150º. The simulated peak positions reproduced the m ones. The value of the R_F calculated to be 0.48 by Eq. (6), which was higher than that of the single-crystals. However, this value was same level compared with the reported value of the previous study by using the highly oriented thin film [26]. In general, the single-crystal X-ray structure analysis is carried out at the lower temperature than the room temperature for the suppression of the molecular vibration. Wide distribution of the alkyl-chains of $C6PcH_2$ was also obtained at room temperature by the single-crystal X-ray structure analysis [29]. In this study, the GIWAX measurement was carried out at room temperature; therefore, the high R_F should be obtained.

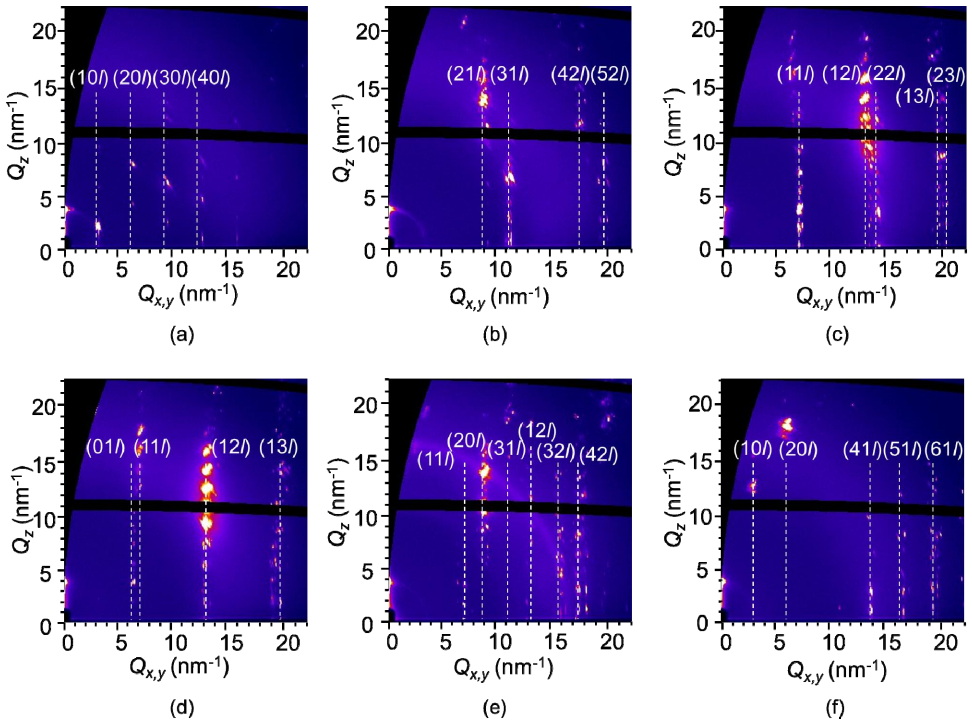

Figure 4. Measured XRD patterns and Miller indices of the thin film when the thin film rotated counterclockwise by (a) 0º, (b) 30º, (c) 60º, (d) 90º, (e) 120º, and (f) 150º. The angle is set to be 0º when the incident X-rays are parallel to the sweep direction of the wire-bar.

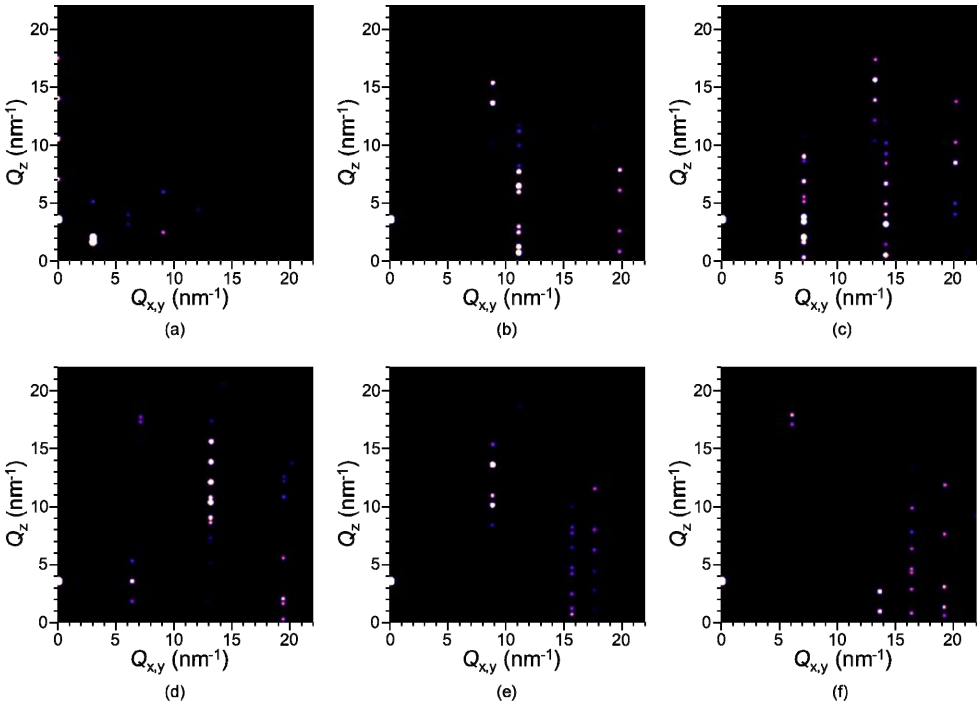

Figure 5. Calculated patterns of the thin film when the thin film rotated counterclockwise by (a) 0º, (b) 30º, (c) 60º, (d) 90º, (e) 120º, and (f) 150º. The angle is set to be 0º when the incident X-rays are parallel to the *a* axis of the single-crystal structure of $C6PcH_2$.

The molecular orientation distribution in the azimuthal direction was evaluated by the X-ray rocking curve. Figure 6 shows the rocking curves of the (101) plane of $C6PcH_2$ in the bar-coated thin film. The intensity was calculated by the integration of intensity in the area around the peak position of the (101) plane, which is ($Q_{x,y}$, Q_z) = (3.13, 2.07) (nm^{-1}). Many peaks appeared at the position of φ = 169-178º and 349-358º. The intersection points of the (101) plane and Ewald sphere are calculated to be 178.6 and 358.6º by Eq. (5). The calculated values of φ were consistent with the measured ones within the accuracy of the experimental. The peak width of the rocking curve was approximately 8-9º, and the number of XRD peaks were seven, as shown the arrows in Fig. 6(b). The peak width and number of the peaks represent the distribution in the azimuthal direction and the number of the domains with different orientation at the irradiation area of X-rays, respectively. The irradiation area of X-rays was approximately 40 μm × 1 cm; therefore, seven domains with different orientation must exist in the area.

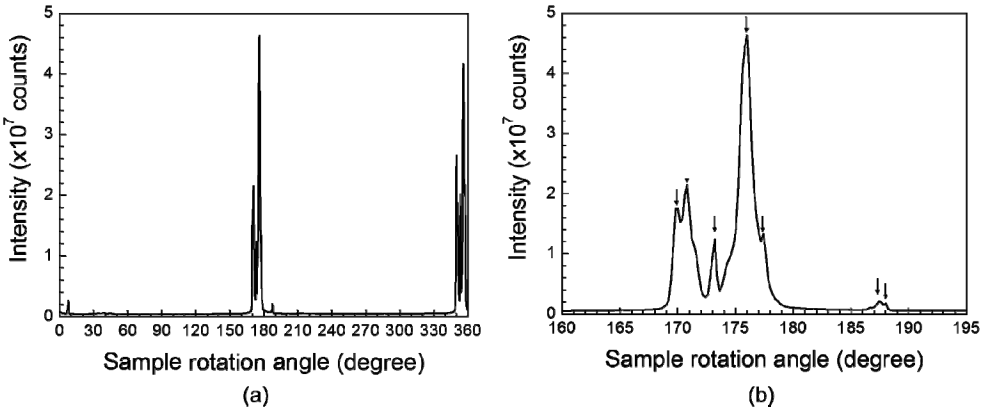

Figure 6. Rocking curve of the (101) plane of $C6PcH_2$ in the bar-coated thin film. Sample rotation angles are in ranges (a) 0-360º and (b) 160-195º. Arrows in Fig. 6(b) represent the XRD peaks.

The distribution of the lattice plane in the azimuthal direction can be obtained by the X-ray rocking curve measurement. While, R_F represents the difference between the measured and calculated intensity of the XRD peaks. The difference originates from the deviation between the practical and assumed atom positions in the crystal lattice. In the case of low R_F, the assumed crystal structure is close to the practical one. From these results, a certainty of the assumed 3D molecular packing structure can be evaluated by the GIWAXS measurement with the sample rotation.

3.2 Homeotropic alignment

In order to realize homeotropic alignment in thin film, a homeotropic alignment process was carried out. Figure 7 shows the schematic diagrams of the molecular orientation in the thin film of $C6PcH_2$ in the homeotropic alignment process, which was divided into a four steps: (i) the film state spin-coated as grown, (ii) covered with the PVP layer, (iii) heated to 175 ºC in the isotropic phase of $C6PcH_2$ and then set at 160 ºC, and (iv) cooled down to set at room temperature. Figure 8 shows the XRD patterns obtained by the GIWAXS measurement in each fabrication step.

The XRD pattern of the sample in the first step is shown in Fig. 8(a). Many arc-shaped peaks were detected in the diffraction image. The distribution of the XRD peaks was wide compared to that in Fig. 4, i.e., the molecular orientation in the spin-coated thin film is disordered compared to that in the bar-coated thin films as mentioned above. A relatively high peak was obtained at ($Q_{x,y}$, Q_z) = (0, 3.60) (nm^{-1}) (17.5 Å). The peak corresponds to the (002) plane of $C6PcH_2$, i.e., the (002) plane is parallel to the glass substrate. Relatively high peaks were obtained at ($Q_{x,y}$, Q_z) = (12.87, 8.47) (nm^{-1}) (4.08 Å) and (12.93, 11.33) (nm^{-1}) (3.65 Å). The peaks correspond to the (125) and (12-6) planes of $C6PcH_2$, respectively. These results are in good agreement with the reported molecular packing structure in the spin-coated thin film of $C6PcH_2$ [11], and the planar orientation should be induced in the spin-coated thin film, as shown in Fig. 7(a).

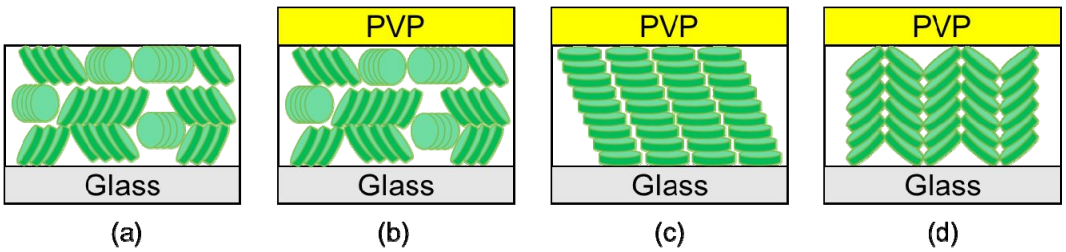

Figure 7. Schematic diagrams of (a) the $C6PcH_2$ spin-coated thin film as grown, (b) the $C6PcH_2$ thin film covered with a PVP layer, (c) the $C6PcH_2$ thin film covered with the PVP layer at 160 ºC, and (d) the $C6PcH_2$ thin film covered with the PVP layer after thermal treatment.

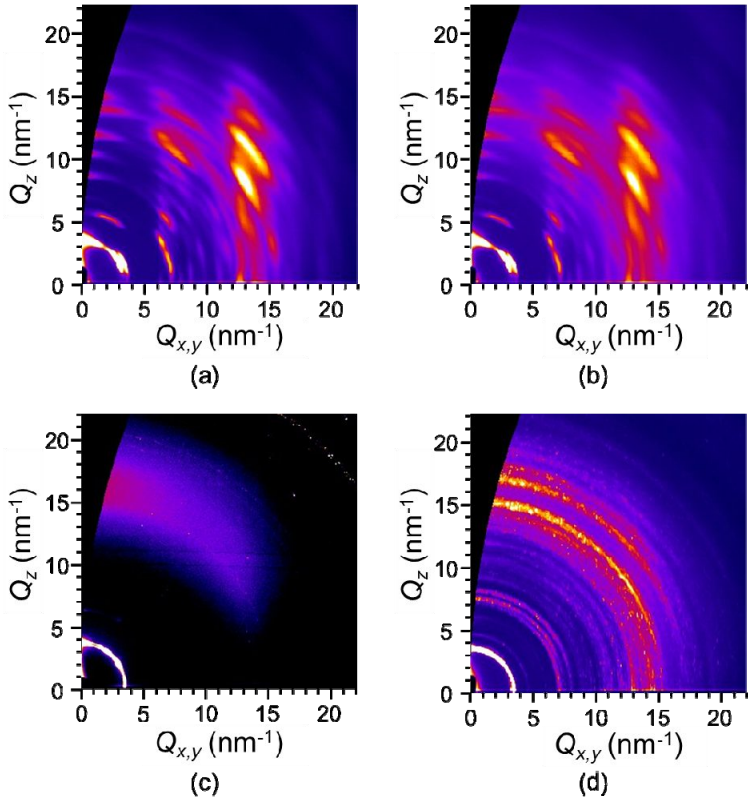

Figure 8. XRD patterns of (a) the $C6PcH_2$ spin-coated thin film as grown, (b) the $C6PcH_2$ thin film covered with a PVP layer, (c) the $C6PcH_2$ thin film covered with the PVP layer at 160 ºC, and (d) the $C6PcH_2$ thin film covered with the PVP layer after thermal treatment. The cooling rate from 175 ºC to room temperature was 10 ºC/min, and the measurements for (a), (b), and (d) were carried out at room temperature.

The XRD pattern of the sample in the second step is shown in Fig. 8(b). The pattern was almost the similar to that in Fig. 8(a), which indicates that the molecular packing structure and molecular alignment in the $C6PcH_2$ layer unchanged after coating the PVP layer as shown in Fig. 7(b), and that the diffraction originating from the PVP layer was too weak to recognize.

The XRD pattern of the sample in the third step is shown in Fig. 8(c). The XRD pattern significantly changed, and a broad and arc-shape XRD peak was appeared at approximately Q_z = 17.13 nm^{-1} (3.67 Å) in the out-of-plane direction. The broad and arc-shape XRD peak should correspond to the inter-molecular distance of $C6PcH_2$ in the LC

phase. The relatively high intensity in the out-of-plane direction shows the face-on alignment of $C6PcH_2$ in the thin film, and the broad pattern in wavenumber space indicates the distribution of the periodicity. $C6PcH_2$ has been reported to form the pseudo-disordered columnar mesophase in the LC phase [10],[30]. The reported results are consistent with the results in this study. The homeotropic alignment of $C6PcH_2$ in the thin film is induced in the third step as shown in Fig. 7(c).

The XRD pattern of the sample in the fourth step is shown in Fig. 8(d). The circular XRD peak was detected at $|Q|$ = 15.24 nm^{-1} (4.12 Å) and 17.31 nm^{-1} (3.63 Å), which correspond to the (125) and (12-6) plane of $C6PcH_2$, respectively, i.e., diffraction based on the inter-molecular interval. Here, $|Q|$ is wavenumber calculated by the equation: $|Q| = \sqrt{Q_{x,y}^2 + Q_z^2}$. The diffraction intensity in the out-of-plane direction was much higher than that in the in-plane direction. The result shows that the homeotropic alignment in the thin film remained in the crystal phase. Moreover, the strong and circular XRD peak was detected at |Q| = 3.60 nm^{-1} (17.4 Å), which correspond to the (002) plane of $C6PcH_2$. From these results, the molecular packing structure in the thin film should be consistent to the single-crystal structure of $C6PcH_2$. The schematic diagram of the molecular alignment in the thin film is shown in Fig. 7(d). Molecules of $C6PcH_2$ tilt alternately and form herringbone-like structure in the crystal phase [28]. While, molecules of $C6PcH_2$ tilt in the same direction in the LC phase [10],[30]. In other words, the molecular packing structure changed by the cooling process. The change may cause the wide distribution of the molecular orientation in the thin film.

Eventually, the homeotropic alignment of $C6PcH_2$ in the thin film was realized by the fabrication process adopted in this study. However, the distribution of the molecular alignment in the thin film still remains to be broad. For obtaining the thin film with the uniform molecular alignment, the optimization of the conditions of the fabrication process, such as the covered-layer polymer material and cooling rate, should be needed.

4. CONCLUSIONS

Uniaxially planar alignment of $C6PcH_2$ in the thin film was realized by bar-coating at an area of 1 mm^2. The 3D molecular packing structures in the thin films were clarified by the GIWAXS technique with sample rotation. The XRD patterns were reproduced by the simulation utilizing the single-crystal structure of $C6PcH_2$. The parameter R_F, which represents the difference between measured and calculated peak intensity, was introduced, and the certainty of the atom positions in the crystal lattice can be evaluated using R_F. Homeotropic alignment of $C6PcH_2$ in the thin film was also realized by the thermal annealing of the $C6PcH_2$ thin film covered with the PVP layer. The molecular alignment in the thin film was clarified by the temperature-controlled GIWAXS technique. Homeotropic alignment in the thin film was induced in the LC phase, and the molecular alignment was maintained at room temperature in the crystal phase.

5. ACKNOWLEDGMENTS

The XRD measurement in BL19B2 beamline at SPring-8 was carried out by the cooperation with Prof. Masakazu Nakamura, Prof. Hirotaka Kojima, and Dr. Ryo Abe in Nara Institute of Science and Technology. We thank Dr. Tomoyuki Koganezawa in Japan Synchrotron Radiation Research Institute for helpful suggestions about the analysis of the XRD patterns. This work was partially supported by the Advanced Low Carbon Technology Research and Development Program from the Japan Science and Technology Agency and the JSPS KAKENHI Grant Numbers 15H03552, 17K18882, 24246009, and 26600073, and a Grant-in-Aid for JSPS Fellows (No. 15J00448), and Photonics Advanced Research Center at Osaka University.

REFERENCES

[1] Piechocki, C., Simon, J., Skoulios, A., Guillon, D. and Weber, P., "Discotic mesophases Obtained from Substituted Metallophthalocyanines. Toward Liquid Crystalline One-Dimensional Conductors," J. Am. Chem. Soc. 104, 5245-5247 (1982).

[2] Mativetsky, J. M., Wang, H., Lee, Whittaker-Brooks, L. and Loo, Y., "Face-on stacking and enhanced out-of-plane hole mobility in graphene-templated copper phthalocyanine," Chem. Commun. 50, 5319-5321 (2014).
[3] Tang, C. W., "Two-layer organic photovoltaic cell," Appl. Phys. Lett. 48, 183-185 (1986).
[4] Sakai, K. and Hiramoto, M., "Efficient Organic p-i-n Solar Cells Having Very Thick Codeposited i-Layer Consisting of Highly Purified Organic Semiconductors," Mol. Cryst. Liq. Cryst. 491, 284-289 (2008).
[5] Li, L., Tang, Q., Li, H., Yang, X., Hu, W., Song, Y., Shuai, Z., Xu, W., Liu, Y. and Zhu, D., "An Ultra Closely π-Stacked Organic Semiconductor for High Performance Field-Effect Transistors," Adv. Mater. 19, 2613-2617 (2007).
[6] Diao, Y., Shaw, L., Bao, Z. and Mannsfeld, S. C. B., "Morphology control strategies for solution-processed organic semiconductor thin films," Energy Environ. Sci. 7, 2145-2159 (2014).
[7] Cook, M. J., "Properties of Some Alkyl Substituted phthalocyanines and Related Macrocycles," Chem. Rec. 4, 225-236 (2002).
[8] Cherodian, A. S., Davies, A. N., Richardson, R. M., Cook, M. J., Mckeown, N. B., Thomson, A. J., Feijoo, J., Ungar, G. and Harrison, K. J., "Mesogenic Behaviour of some 1,4,8,11,15,18,22,25-Octaalkyl-phathalocyanines," Mol. Cryst. Liq. Cryst. 196, 103-114 (1991).
[9] Iino, H., Hanna, J., Bushby, R. J., Movaghar, B., Whitaker, B. J. and Cook, M. J., "Very high time-of-flight mobility in the columnar phases of a discotic liquid crytal," Appl. Phys. Lett. 87, 132102 (2005).
[10] Miyake, Y., Shiraiwa, Y., Okada, K., Monobe, H., Hori, T., Yamasaki, N., Yoshida, H., Cook, M. J., Fujii, A., Ozaki, M. and Shimizu, Y., "High Carrier Mobility up to 1.4 $cm^2 \cdot V^{-1} \cdot s^{-1}$ in Non-Peripheral Octahexyl Phthalocyanine," Appl. Phys. Express 4, 021604 (2011).
[11] Ohmori, M., Higashi, T., Fujii, A. and Ozaki, M., "Molecular Packing Structure of Mesogenic Octa-Hexyl Substituted Phthalocyanine Thin Film by X-ray Diffraction Analysis," J. Nanosci. Nanotechnol. 16(4), 3318-3321 (2016).
[12] Hori, T., Miyake, Y., Yamasaki, N., Yoshida, H., Fujii, A., Shimizu, Y. and Ozaki, M., "Solution Processable Organic Solar Cell Based on Bulk Heterojunction Utilizing Phthalocyanine Derivative," Appl. Phys. Express 3(10), 101602 (2010).
[13] Dao, Q. D., Hori, T., Fukumura, K., Masuda, T., Kamikado, T., Fujii, A., Shimizu, Y. and Ozaki, M., "Effects of processing additives on nanoscale phase separation, crystallization and photovoltaic performance of solar cells based on mesogenic phthalocyanine," Org. Electron. 14, 2628-2638 (2013).
[14] Yoneya, M., Miyamoto, A., Shimizu, Y., Fujii, A. and Ozaki, M., "Origin of the High Carrier Mobilities of Nonperipheral Octahexyl Substituted Phthalocyanine," J. Phys. Chem. 119(42), 23852-23858 (2015).
[15] Yoneya, M., Miyamoto,, A., Shimizu, Y., Ohmori, M., Fujii, A. and Ozaki, M., "Characterization of crystal polymorphs of the organic semiconductor non-peripheral octa-hexyl phathalocyanine," Jpn. J. Appl. Phys. 56, 081601 (2017).
[16] Ohmori, M., Nakatani, M., Kajii, H., Miyamoto, A., Yoneya, M., Fujii, A. and Ozaki, M., "Fabrication of field-effect transistor utilizing oriented thin film of octahexyl-substituted phthalocyanine and its electrical anisotropy based on columnar structure," Jpn. J. Appl. Phys. 57, 03EH10 (2018).
[17] Higashi, T., Ramananarivo, M. F., Ohmori, M., Yoshida, H., Fujii, A. and Ozaki, M., "Polymer blend effects on fundamental properties of mesogenic phthalocyanine films fabricated by heated spin-coating method," Jpn. J. Appl. Phys. 54, 04DK08 (2015).
[18] Higashi, T., Ramananarivo, M. F., Ohmori, M., Yoshida, H., Fujii, A. and Ozaki, M., "Macroscopically aligned molecular stacking structures in mesogenic phthalocyanine derivative films fabricated by heated spin-coating method," Thin Solid Films 594(2), 1-4 (2015).
[19] Ramananarivo, M. F., Higashi, T., Ohmori, M., Sudoh, K., Fujii, A. and Ozaki, M., "Uniaxial crystal growth in thin film by utilizing super cooled state of mesogenic phthalocyanine," Appl. Phys. Express 9(6), 061601 (2016).
[20] Kitagawa, T., Ramananarivo, M. F., Fujii, A. and Ozaki, M., "Polymer Blend Effect on Molecular Alignment Induce by Contact Freezing of Mesogenic Phthalocyanine," Jpn. J. Appl. Phys., in press.
[21] Pisula, W., Menon, A., Stepputat, M., Lieberwirth, I., Kolb, U., Tracz, A., Sirringhaus, H., Pakula, T. and Müllen, K., "A zone-casting technique for device fabrication of field-effect transistors based on discotic hexa-peri-hexabenzocoronene," Adv. Mater. 17(6), 684-689 (2005).
[22] Usui, T., Nakata, Y., Banoukepa, G. D. R., Fujita, K., Nishikawa, Y., Shimizu, Y., Fujii, A. and Ozaki, M., "Glass-sandwich-type organic solar cells utilizing liquid crystalline phthalocyanine," Appl. Phys. Express 10(2), 021602 (2017).

[23] Nakata, Y., Usui, T., Nishikawa, Y., Nekelson, F., Shimizu, Y., Fujii, A. and Ozaki, M., "Sandwich-cell-type bulk-heterojunction organic solar cells utilizing liquid crystalline phthalocyanine," Jpn. J. Appl. Phys. 57, 03EJ03 (2018).
[24] Cupere, V. D., Tant, J., Viville, P., Lazzaroni, R., Osikowicz, W., Salaneck, W. R. and Greerts, Y. H., "Effect of interfaces on the alignment of a discotic liquid-crystalline phthalocyanine," Langmuir 22(18), 7798-7806 (2006).
[25] Pouzet, E., Cupere, V. D., Heintz, C., Andreasen,, J. W., Breiby, D. W., Nielsen, M. M., Viville, P., Lazzaroni, R., Gbabode, G. and Geerts, Y. H., "Homeotropic alignment of a discotic liquid crystal induced by a sacrificial layer," J. Phys. Chem. C 113(32), 14398-14406 (2009).
[26] Watanabe, T., Koganezawa, T., Kikuchi, M., Videlot-Ackermann, C., Ackermann, J., Brisset, H., Hirosawa, I. and Yoshimoto, N., "Crystal structure of oligothiophene thin films characterized by two-dimensional grazing incidence X-ray diffraction," Jpn. J. Appl. Phys 53, 01AD01 (2013).
[27] Swarts, J. C., Langner, E. H. G., Krokeide-Hove, N. and Cook, M. J., "Synthesis and electrochemical characterization of some long chain 1,4,8,11,15,18,22,25-octa-alkylated metal-free and zinc phthalocyanines possessing discotic liquid crystalline properties," J. Mater. Chem. 11, 434-443 (2001).
[28] Ohmori, M., Nakano, C., Miyano, T., Tohnai, N., Fujii, A. and Ozaki, M., "Single crystal growth and X-ray structure analysis of non-peripheral octahexyl phthalocyanine," J. Cryst. Growth 445, 9-14 (2016).
[29] Ohmori, M., Nakano, C., Fujii, A., Shimizu, Y. and Ozaki, M., "Selective crystal growth of polymorphs and crystal-to-crystal thermal phase transition of non-peripherally alkyl-substituted phthalocyanine and tetrabenzotriazaporpphyrin," J. Cryst. Growth 468, 804-809 (2017).
[30] Nakagawa, D., Nakano, C., Ohmori, M., Itani, H., Shimizu, Y., Fujii, A. and Ozaki, M., "Miscibility and carrier transport properties in binary blend system of non-peripherally octa-hexyl-substituted phthalocyanine analogues," Org. Electron. 44, 67-73 (2017).